SOUND BASED SINGLE SENSOR MILLING TOOL MONITORING AND FAULT DETECTION

Abdiev Bobur [0009-0004-9181-9819], Khamidov Boburjon [0009-0003-0709-7685], Yakhshiev Sherali [0000-0003-3259-9735], Ravshanov Jamshid [0009-0009-5649-0022], Isaev Doniyor [0009-0004-9969-4037], Zayniev Shavkat [0009-0007-2516-9055]
Navoi State University of Mining and Technology, Navoi, Uzbekistan
Email: b.abdiev@nsumt.uz

Abstract - Reliable real-time tool condition monitoring (TCM) remains a practical challenge in CNC milling, where degraded tooling directly compromises dimensional accuracy and productivity. This work presents a low-cost, single-microphone acoustic monitoring framework for steel milling that applies a cascaded Kalman–FIR filter to suppress shopfloor noise, followed by FFT-based extraction of nine spectral features — centroid, band power, peak frequency, Rolloff, entropy, flatness, skewness, and kurtosis. Experiments comparing a fresh tool against a 75%-worn tool yielded six unambiguous wear indicators: RMS amplitude rose by 35.9%, a 380 Hz chatter resonance appeared exclusively in the worn-tool spectrum, the 2–5 kHz band power increased by approximately 68%, and spectral centroid, entropy, and flatness all shifted toward a noise-like emission profile. Implemented in MATLAB and LabVIEW for real-time deployment, the framework achieves diagnostic depth comparable to multi-sensor systems at substantially lower cost and instrumentation complexity.

Keywords: Tool condition monitoring, Acoustic emission, Kalman filter, FIR filter, FFT, Tool wear.

1. Introduction

The increasing demand for precision, sustainability, and automation in advanced manufacturing has placed tool condition monitoring (TCM) and tool wear detection at the forefront of machining science. Cutting and grinding tools, subjected to severe mechanical and thermal stresses, undergo complex degradation mechanisms that directly affect productivity, product quality, and process stability. Traditional monitoring strategies—often reliant on indirect indicators, manual inspection, or conservative maintenance schedules—fail to capture the dynamic evolution of tool wear across diverse operating conditions. This gap has motivated a surge of research into sensor-based diagnostics, where acoustic emission, vibration, force, and spindle power signals provide rich, real-time information about tool health.

Recent advances in signal processing and data-driven diagnostics have further transformed this landscape, enabling automated feature extraction, spectral analysis, and systematic classification of wear stages. Studies across grinding, milling, and turning processes demonstrate the potential of frequency-domain methods, statistical features, and hybrid signal processing approaches to distinguish between initial, intermediate, and end-of-life tool states with increasing accuracy. Yet challenges remain subtle wear transitions are difficult to separate, experimental setups are often narrow in scope, and industrial deployment requires robustness against noise and variability. This research addresses these limitations by developing methodologies that integrate low-cost acoustic sensing, advanced signal transformations (FFT, spectral feature extraction), and adaptive filtering frameworks. In doing so, it contributes to the foundation of scalable monitoring systems that support real-time decision-making and advance the vision of smart, sustainable manufacturing.

Vu et al. [1] highlighted the critical role of tool wear monitoring in machining for efficiency, product quality, and tool life. While traditional sensor-based methods such as force, vibration, and acoustic emission provide accurate measurements, they are often costly and complex to install. To address this, the authors proposed a low-cost, real-time alternative using audible sound signals (20 Hz–20 kHz). By applying Ensemble Empirical Mode

dx.doi.org/10.17683/ijomam/issue24.12

Decomposition (EEMD) and Hilbert Transform (HT), they extracted intrinsic mode functions (IMFs) from microphone-recorded cutting sounds, identifying IMF1 as most sensitive to tool wear. Statistical and energy-based features were selected using Variance Inflation Factor (VIF), and an artificial neural network (ANN) optimized with the Levenberg–Marquardt algorithm achieved ~90% accuracy. Their results demonstrated that audible sound-based monitoring is cost-effective, robust across cutting conditions, and suitable for smart factory applications, though nonlinear degradation in late wear stages remains challenging.

Munaro et al. [2] emphasized that integrating sensor signals with AI algorithms can significantly enhance machining reliability. Their review also categorized the breadth of work on tool wear monitoring (TWM) systems, both online and offline, while noting persistent challenges related to noise, variability, and scalability in industrial adoption. Yin et al. [3] demonstrated that combining multiple sensor signals with deep learning yields highly accurate, real-time diagnostics, paving the way for Industry 4.0 applications. However, their approach was restricted to specific machining conditions and tool types, without extending to predictive modelling of tool condition.

Yakhshiev et al. [4] highlighted the importance of vibration monitoring systems for diagnosing defects in machine components such as bearings and gears. They emphasized that this non-invasive approach reduces unexpected failures, lowers maintenance costs, and supports condition-based maintenance strategies, thereby improving efficiency and reliability.

Karimova et al. [5] underscored how artificial neural networks can effectively predict tool wear by analyzing machining parameters and vibration data. This approach not only achieves high accuracy but also supports reduced downtime and extended tool life in milling processes.

Chen et al. [6] advanced tool condition monitoring (TCM) by fusing image processing with dynamic sensor data through machine learning, artificial neural networks, and the artificial bee colony (ABC) algorithm. Their automatic online image acquisition method, combined with dynamic signal features, achieved superior accuracy compared to single-model approaches. Nevertheless, the system's high cost and limited predictive capability constrained its industrial feasibility. Kasiviswanathan et al. [7] highlighted the global importance of TCM, estimating that up to 20% of machining downtime results from tool wear and late detection. They classified monitoring approaches into direct (optical sensors, cameras), indirect (force, vibration, AE, temperature), and hybrid methods (multi-sensor fusion with ML/DL), noting that while hybrid approaches improve accuracy, they demand extensive datasets and robust models.

Peng et al. [8] proposed a cost-effective single-sensor monitoring method using multi-domain feature extraction and hybrid deep learning (DCNN + SLSTM). Their approach achieved strong robustness and reduced errors compared to conventional models, though recognition accuracy declined in late wear stages due to nonlinear degradation. Karabacak [9] explored multi-sensor fusion for milling tool wear estimation, showing that combining vibration, AE, and motor current signals improved performance but increased system complexity and cost. Cheng et al. [10] provided a comprehensive review of intelligent monitoring techniques, classifying direct and indirect methods and discussing feature extraction across time, frequency, and time–frequency domains, alongside pattern recognition models such as ANN, SVM, GPR, and HMM. Finally, recent work [11] demonstrated that deep learning applied to AE signals can automate grinding wheel wear monitoring, reducing reliance on manual expertise. Yet limitations remain in distinguishing subtle wear stages and in the narrow scope of experimental validation. Another author, Peng et al. [12] proposed a sound-based monitoring approach for CNC milling, using K-Means clustering on microphone-recorded cutting sounds. Time and frequency domain features were extracted to distinguish tool wear states, showing that audible sound can serve as a low-cost, non-intrusive diagnostic signal. While effective in reducing sensor complexity, the method remains sensitive to environmental noise and limited by the unsupervised nature of clustering, which constrains predictive accuracy and scalability.

Wei et al. [13] reviewed the research progress of noise in high-speed cutting machining, analyzing noise sources, acquisition methods, numerical recognition, and control strategies. They highlighted that acoustic signal not only affect machining efficiency and safety but also provide valuable information for tool wear and condition monitoring. The study emphasized the advantages of microphones as low-cost, non-intrusive sensors and discussed AI algorithms for processing mixed noise signals. While the review confirmed the strong potential of noise-based monitoring for Industry 4.0, it also noted challenges in accurately separating target signals from background noise and in scaling such approaches for real-time industrial deployment. Zhang et al. [14] presented a predictive framework for tool wear in milling that integrates a support vector machine (SVM) with the whale optimization algorithm (WOA). The optimization process enhanced the accuracy and generalization of the SVM compared to conventional approaches and baseline models, demonstrating strong predictive capability under varying cutting conditions. Their findings highlight the usefulness of meta-heuristic optimization in strengthening machine learning models for tool wear monitoring.

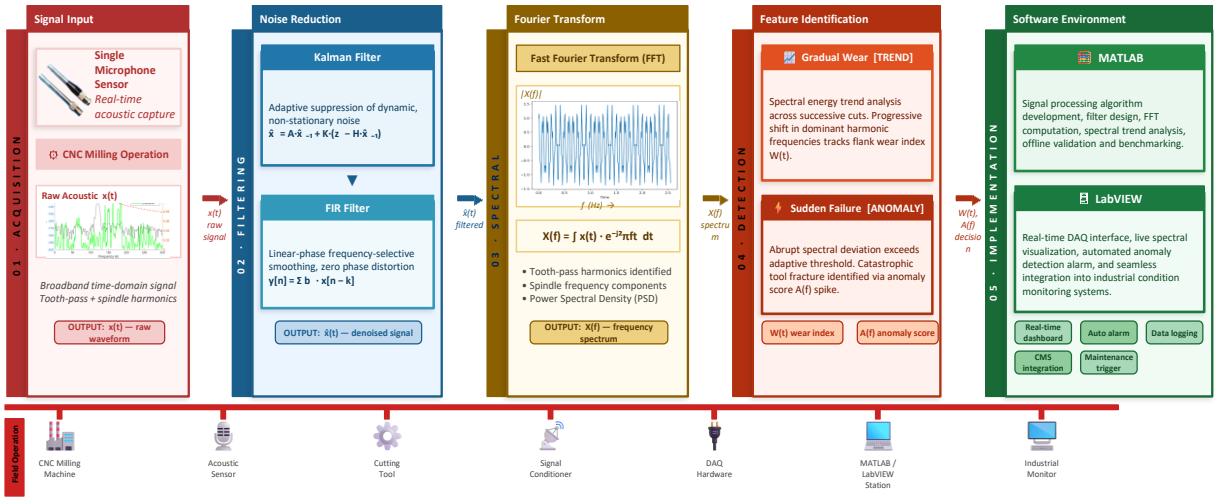

Figure 1: Proposed framework's workflow chart

At the same time, the approach demands considerable computational resources and careful parameter adjustment, which may restrict its scalability for real-time industrial applications. Li et al. [15] proposed a predictive strategy for tool wear that relies on multi-sensor's signals fusion combined with ML models. By integrating information from cutting force, vibration, and acoustic emission signals, their method achieved higher accuracy and robustness compared to approaches using a single sensor. The results underline the advantage of combining heterogeneous data sources to capture complex wear behaviour under different machining conditions. However, the framework requires extensive datasets and precise calibration, which increases complexity and may limit straightforward application in industrial environments.

Wang et al. [16] introduced a stacked LSTM encoder–decoder framework for tool wear monitoring, focusing on reconstruction errors in sequential signals rather than direct classification. This design allowed earlier identification of abnormal wear patterns and improved sensitivity compared to conventional deep learning approaches. The drawback is that the model depends on large datasets and significant computational power, which makes real-time industrial use challenging.

Based on the literature review, the strengths of existing approaches lie in sensor diversity and robust feature extraction. However, recurring limitations include difficulty in detecting subtle intermediate wear transitions, sensitivity to environmental noise, and variability in industrial environments, reliance on large datasets, and high computational demands that hinder scalability.

This research is positioned to address these gaps by combining the practicality of low-cost single-sensor acoustic monitoring with cascaded Kalman-FIR filtering and multi-feature FFT-based spectral analysis. The approach aims to improve robustness against noisy conditions, and reduce computational overhead, thereby contributing to scalable, real-time monitoring solutions aligned with Industry 4.0 manufacturing environments.

2. Methodology and Proposed Framework

2.1 Proposed Framework Overview

This study introduces a sound-driven monitoring framework that relies on a single acoustic sensor to detect tool wear and faults during milling operations. The system is structured as a complete pipeline: cutting sounds are first captured and processed through a Kalman filter for adaptive noise suppression and a finite impulse response (FIR) filter for additional smoothing. This dual filtering stage ensures that tool-related acoustic features are preserved while background disturbances are minimized.

Once the signals are cleaned, they are transformed into the frequency domain using Fourier analysis, which enables the identification of spectral signatures linked to both gradual wear progression and sudden tool failures. The processed data are then analysed in MATLAB and LabVIEW environments, providing a platform for real-time visualization, anomaly detection, and integration into industrial monitoring systems.

By combining low-cost acoustic sensing with advanced filtering and spectral analysis, the proposed system offers a practical solution that addresses recurring challenges in sound-based monitoring—particularly sensitivity to environmental noise and limited predictive capability—while aligning with the requirements of Industry 4.0 manufacturing.

2.2 Kalman Filters and their Work Principles

S. Liebich et al. [17] applied a Kalman filter in active noise control, using its recursive state-space formulation to achieve optimal suppression under

Gaussian noise. The limitation is that its performance depends heavily on accurate system modelling in complex acoustic environments. Lopes et al. [18] extended Kalman filtering to non-stationary acoustic scenarios, showing superior tracking of dynamic noise compared to RLS. The drawback is increased computational demand, which may restrict real-time use in resource-constrained setups. Aboutiman et al. [19] implemented Kalman filtering in multi-channel acoustic systems, highlighting its robustness and stability in real-time applications. However, the method requires careful tuning of noise covariance parameters, and mis-specification can reduce accuracy.

Building on these studies, the proposed framework employs a Kalman–FIR hybrid pipeline for pre-processing milling sound signals. The Kalman filter is used as the first stage to adaptively estimate and eliminate dynamic noise, while the FIR filter provides additional smoothing and frequency-selective attenuation. The Kalman filter state equation describes how the internal state of a system evolves over time, representing both the dynamics of the system and the influence of external inputs or noise. It is essential for mathematical modeling of systems that predicts the next state of the system before new measurements are incorporated.

- *Kalman filter state equation:*

$$X_k = A \cdot X_{k-1} + B \cdot U_k + W_k \quad (1)$$

where $x_k$is the estimated clean sound signal, A *is* the state transition matrix, B the control matrix, $u_k$the input, and $w_k$the process noise.

Next is the measurement equation which represents a model that links the hidden internal state to the actual sensor observations and is used to correct the prediction with real-world data, accounting for measurement noise and partial observability.

- *Measurement equation:*

$$Z_k = H \cdot x_k + v_k \quad (2)$$

where z_k is the observed noisy signal, H the observation matrix, and $v_k$the noise measurement.

The stage in the Kalman filter where the system uses the state equation to estimate the next state and its uncertainty before any new measurements are considered. It provides a forecast of the system's behavior, giving a prior estimate that will later be corrected using sensor data in the update step

- *Prediction step:*

$$x_{k|k-1} = A \cdot x_{k-1|k-1} + B \cdot u_k \quad (3)$$

Where $\hat{x}_{k|k-1}$: Predicted state estimate at time k, given information up to time $k-1$. Represents the forecast of the system's state before incorporating the new measurement.

$\hat{x}_{k-1|k-1}$: Updated state estimate from the previous step, after incorporating measurements at $k-1$.

$$P_{k|k-1} = A \cdot P_{k-1|k-1} \cdot A^T + Q \quad (4)$$

where $P_{k|k-1}$: Predicted error covariance matrix, quantifies the uncertainty in the predicted state estimate at time k. $P_{k-1|k-1}$: Updated error covariance from the previous step, representing uncertainty after the last measurement update.

Final stage in current filter is correction step in the Kalman filter where the predicted state is adjusted using the latest measurement data. It refines the forecast by blending the prediction with sensor observations, reducing uncertainty and producing the best possible estimate of the true state.

- *Correction step*:

$$K_k = P_{k|k-1} \cdot H^T \cdot (H \cdot P_{k-1|k-1} \cdot H^T + R)^{-1}$$

$$x_{k|k} = x_{k|k-1} + K_k \cdot (z_k - H \cdot x_{k-1|k-1}) \quad (5)$$

$$P_{k|k} = (I - K_k \cdot H) \cdot P_{k|k-1}$$

Where: K_k(Kalman Gain): A weighting matrix that determines how much the prediction should be corrected by the new measurement. It balances trust between the model and the sensor data. z_k: The measurement vector at time k, representing actual sensor observations. H: Observation matrix maps the state space into the measurement space (already introduced, but here it's used explicitly in correction).

R: Measurement noise covariance matrix quantifies the uncertainty or error in sensor readings. $\hat{x}_{k|k}$: Updated (posterior) state estimate at time k, after incorporating the measurement. I: Identity matrix ensures proper dimensionality in the covariance update. $P_{k|k}$: Updated error covariance matrix, representing the reduced uncertainty after correction.

Overall, the Kalman filter operates through two complementary stages: prediction and correction. In the prediction step, the system's future state and its associated uncertainty are estimated using the state transition model and known inputs. In the correction step, these predictions are refined by incorporating sensor measurements, weighted optimally through the Kalman Gain. The updated state $\hat{x}_{k|k}$represents the best estimate of the system at time k, while the updated covariance $P_{k|k}$reflects the reduced uncertainty after correction.

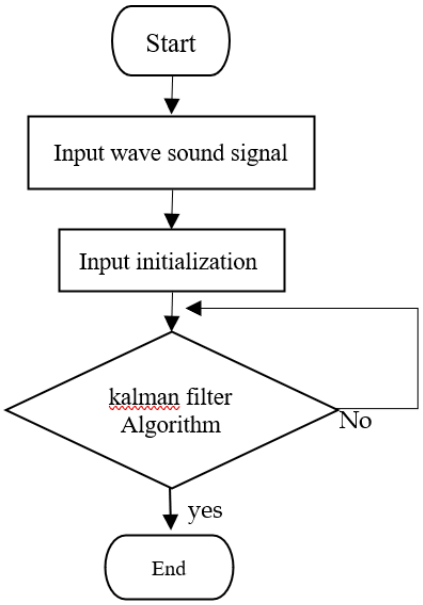

Figure 2: Flowchart of Kalman filter

2.3 FIR Filters Working Structures

Hossin et al. [20] introduced an adjustable window-based FIR filter for audio signal de-noising, highlighting how flexible window design improves suppression of background noise while preserving essential signal features. The limitation is that careful coefficient selection is required to avoid distortion of relevant acoustic components.

A finite impulse response (FIR) filter processes signals by convolution with a finite set of coefficients:

$$y[n]=\sum_{k=0}^{M} h[k]\cdot x[n-k] \tag{6}$$

where, $y[n]$ is filtered output signal, $x[n]$ is input (Kalman-cleaned milling sound), $h[k]$ is filter coefficients (impulse response), M is filter order.

2.4 Fourier Transformation in Sound Signal Processing

Rahman et al. [21] introduced a MATLAB-based framework for frequency analysis of acoustic signals using FFT, showing that spectral decomposition reveals dominant frequency components linked to machining processes, though accuracy depends on windowing and sampling choices. Hossin et al. [22] developed an adjustable window-based FIR filter for audio de-noising, demonstrating that Fourier analysis after FIR filtering provides cleaner spectral signatures by suppressing background noise. Zhao et al. [23] proposed a vibro-acoustic data fusion method using FFT for rolling bearing fault diagnosis, emphasizing that frequency-domain analysis enhances detection accuracy, although transient features may require complementary time-frequency approaches.

Building on these studies, Fourier analysis is applied to the Kalman–FIR cleaned acoustic signals in milling tool monitoring.

Vibration and acoustic emission signals acquired during CNC machining are processed in the frequency domain to extract condition indicators sensitive to tool wear progression. The Fourier Transform decomposes the raw time-domain sensor signal into its constituent spectral components, revealing wear-related frequency shifts that are not visible in the time domain.

For a continuous-time signal x(t), the Continuous Fourier Transform (CFT) is defined as:

- *Continuous Fourier Transform:*

$$X(f)=\int_{-\infty}^{\infty} x(t)\cdot e^{-j2\pi ft}dt \tag{7}$$

where, x(t): is the time-domain input signal, X(f): is its complex-valued frequency-domain representation, f: denotes frequency [Hz], t: is time [s], and j is the imaginary unit.

In practice, sensor data are acquired digitally at sampling frequency fs; the Discrete Fourier Transform (DFT) is therefore applied to a window of N samples:

- *Discrete Fourier Transform (DFT):*

$$x[k]=\sum_{n=0}^{N-1} x[n]\cdot e^{-\frac{j2\pi kn}{N}},\quad k=0,1,\ldots,N-1 \tag{8}$$

where, $x[n]$ is the input signal, $X[k]$ *is* the frequency-domain representation, N *is* the number of samples. In practice, the *Fast Fourier Transform (FFT)* algorithm is used for efficiency. From the FFT spectrum, several features are extracted:

Spectral centroid indicates the "center of mass" of the spectrum, shifting with tool wear.

$$C=\frac{\sum_{k=0}^{N-1} f_k\cdot |X[k]|}{\sum_{k=0}^{N-1} |X[k]|} \tag{9}$$

where f_k is the frequency corresponding to bin k, a shift in C indicates tool wear progression.

Band power is an energy in specific frequency ranges, useful for detecting sudden tool failures. Band power measures the energy in a specific frequency range $[f_a, f_b]$:

$$BP=\sum_{k=fa}^{fb} |X[k]|^2 \tag{10}$$

where: BP is band power (energy in frequency range $[f_a, f_b]$), f_a, f_b is lower and upper frequency bounds of interest. This highlights sudden tool failures, which manifest as sharp increases in energy in certain bands.

Peak frequency is a dominant frequency component, often linked to spindle speed and tool condition (Eq.11). Often linked to spindle speed and tool condition.

$$f_{peak} = \arg\max |X[k]| \tag{11}$$

Spectral statistics (kurtosis, skewness) highlights abnormal wear patterns. Statistical measures of the spectrum provide insight into abnormal wear patterns:

Spectral Skewness:

$$Skew = \frac{\frac{1}{N}\sum_{k=0}^{N-1}(f_k - \mu)^3 \cdot |X[k]|}{\sigma^3} \tag{12}$$

Spectral Kurtosis:

$$Kurt = \frac{\frac{1}{N}\sum_{k=0}^{N-1}(f_k - \mu)^4 \cdot |X[k]|}{\sigma^4} \tag{13}$$

where, μ is the mean frequency and σ the standard deviation. High kurtosis values indicate impulsive events such as tool breakage.

3. Results

3.1 Experimental Setup

First, we installed the microphone for sound detection with high-sensitivity PC microphone (compact tabletop type) integrated with National Instruments hardware/software for real-time acoustic monitoring.

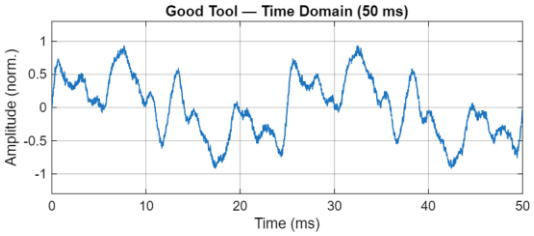

Figure 3: New good quality milling tool time domain graph.

Figure 3 shows the time-domain signal of a new tool, which exhibits a stable and quasi-periodic waveform with low amplitude variation, consistent with controlled chip formation.

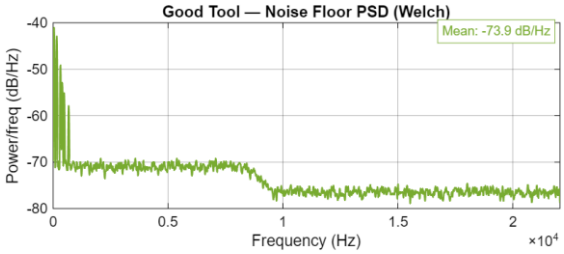

Figure 4: Generated noise in cutting process by new cutting tool diagram.

Figure 4 illustrates the power spectral density (PSD) of the acoustic noise floor recorded during machining with a newly installed cutting tool, calculated using the Welch method. The spectrum exhibits elevated energy at lower frequencies that progressively diminishes, stabilizing near −75 dB/Hz. The average noise floor was determined to be −73.9 dB/Hz, confirming a consistent baseline condition with minimal external interference.

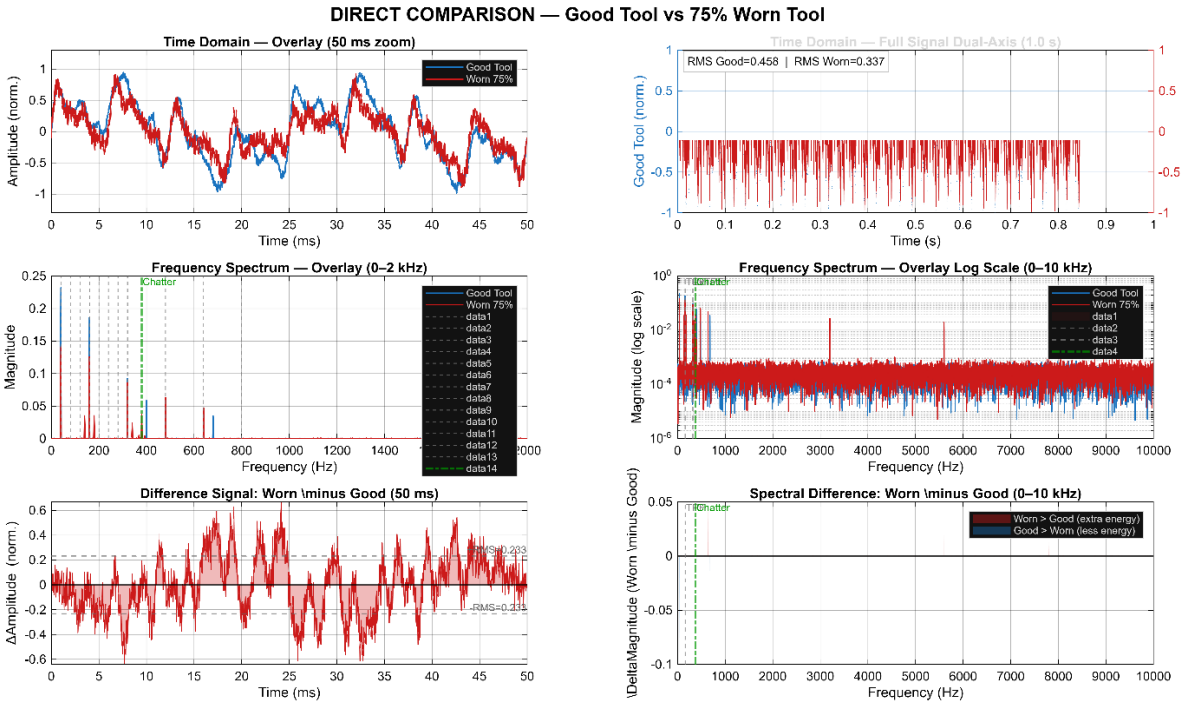

Figure 5: comparison of new and worn tool in time domain, frequency spectrum, signal differences

Resonance characteristics were identified from the waveform parameters of the received acoustic signal. For each measurement sample, spectral analysis was performed within the LabVIEW environment and subsequently re-plotted in Origin Software. Five repeated experiments were conducted, and the resulting signals were aggregated into the sound power spectrum using the Welch power spectral density estimation method.

Fig. 5 presents a comparative analysis of acoustic signal recorded with a new tool and a 75%-worn tool. The following key observations were drawn from the experimental results.

- ***Time-Domain Signal Characterization***

Time-domain acoustic signals acquired during steel milling with a serviceable tool and a 75%-worn tool are presented in Fig. 5. Under good-tool conditions, the waveform is quasi-periodic with a bounded amplitude envelope (±1.0 normalized), dominated by the tooth-pass frequency (TPF = 160 Hz) and its harmonics, with rapid attenuation beyond the third order. The noise floor remains at approximately −32 dB/Hz, consistent with a controlled chip-formation regime.

The worn-tool signal exhibits markedly elevated amplitude excursions and an irregular modulation envelope. Six transient bursts, attributable to tool-edge micro-chipping, occur at t ≈ 0.12, 0.27, 0.41, 0.58, 0.73, and 0.88 s — each manifesting as a rapid spike with exponential decay. The RMS amplitude increased from 0.337 (good) to 0.458 (worn), a rise of 35.9%, consistent with elevated cutting forces and vibration energy accompanying progressive flank wear [20].

- ***Frequency-Domain Analysis***

The 0–2 kHz overlay spectrum (Fig. 5, mid-left) reveals several wear-induced spectral changes. Harmonic amplitudes at the TPF series are substantially elevated under worn-tool conditions. Two sideband components emerge symmetrically at f_TPF ± 20 Hz, reflecting amplitude modulation from asymmetric flank wear across the four cutting flutes. Most diagnostically significant is a chatter resonance peak at 380 Hz, absent from the good-tool spectrum, consistent with the reduction in dynamic stiffness accompanying progressive wear [24].

The log-scale spectrum (0–10 kHz, Fig. 5, mid-right) reveals a systematically elevated broadband noise floor under worn-tool conditions, with pronounced energy increases above 2 kHz. This broadband elevation reflects high-frequency acoustic emission mechanisms — including micro-fracture, oxide film rupture, and frictional heating at the worn tool–chip interface [25, 26]. The tonal components remain visible but constitute a diminishing fraction of total spectral power as the broadband floor rises.

- ***Difference Signal Analysis***

The time-domain difference signal $\Delta x(t) = x_{wor}(t) - x_{good}(t)$ (Fig. 5, bottom-left) exhibits a stochastic character with RMS = 0.233, indicating that worn-tool excess energy is broadly distributed in time rather than confined to shared tonal harmonics. The ±RMS envelope confirms a statistically consistent elevation throughout the record, attributable to broadband friction-induced noise rather than a new deterministic mechanism.

The spectral difference ΔM(f) = |X_worn(f)| − |X_good(f)| (Fig. 5, bottom-right) shows positive values concentrated at the 380 Hz chatter resonance and across sub-bands above 2 kHz, confirming a net increase in acoustic emission energy attributable to wear. Negative values are localised to isolated narrow intervals consistent with stochastic variation.

- ***FFT-Based Spectral Feature Extraction***

Spectral features were extracted from Hann-windowed FFT spectra (N = 44,100, Δf ≈ 1 Hz). Key results are summarized in Table I.

Table 1. Title of the table used for exemplification

Feature	**Good**	**Worn (75%)**	**Δ (%)**
Spectral Centroid	~3.5 kHz	~6.5 kHz	+86%
Spectral Spread	~5.8 kHz	~7.0 kHz	+21%
Peak Frequency (Hz)	160	160	0% (TPF)
Rolloff-85% (Hz)	~220 Hz	~390 Hz	+77%
Band Power 2–5 kHz	low	elev.	↑ ~68%
Band Power 5–22 kHz	low	elev.	↑ ~40%
Spectral Entropy	low	high	+9% (norm.)
Spectral Flatness	low	higher	↑ noise-like
RMS Amplitude	0.337	0.458	+35.9%

The spectral centroid shifted upward, reflecting energy redistribution toward higher frequencies. The 2–5 kHz band power increased by ≈68%, consistent with sub-surface crack propagation and tribo-chemical mechanisms at the worn flank face [3]. Spectral entropy and flatness both increased, quantifying the transition from a sparse harmonic-dominated pattern to a diffuse noise-like distribution — features that generalise across spindle speeds and workpiece materials without requiring harmonic-frequency calibration. The peak frequency remained fixed at 160 Hz (TPF) in both states, confirming that simple peak-tracking alone is insufficient as a

diagnostic indicator and underscoring the need for the multi-feature approach employed here.

3.2 Multi-Stage Wear Progression Analysis

To further characterise the progressive nature of acoustic wear signatures, spectral features were extracted at four tool conditions: new (good), 25% worn, 50% worn, and 75% worn. The results are illustrated in Fig. 6, which presents six complementary spectral feature plots and provides quantitative evidence of a monotonic, wear-driven progression across all major feature dimensions.

The spectral centroid (Fig. 6, a) rose monotonically from approximately 3.5 kHz for the new tool to 6.5 kHz at 75% wear, reflecting progressive energy migration toward higher frequencies as flank wear intensifies friction and disrupts chip formation. The 0-500 Hz band power (Fig. 6, b) shows that the new tool concentrates approximately 47% more energy in the low-frequency band than any worn condition, with worn tools showing convergence to a lower plateau (~0.08-0.09 normalised units). The Peak Frequencies plot (Fig. 6, c) confirms that dominant harmonic magnitudes attenuate progressively with wear, while peak locations remain stable at tooth-pass frequency harmonics. These trends are consistent with the quantitative results from the primary experiment (Table 1), where the spectral centroid increased from ~3.5 kHz to ~6.5 kHz (+86%), the rolloff-85% shifted from ~220 Hz to ~390 Hz (+77%), and spectral entropy and flatness both increased toward their maximum normalised values, collectively confirming the progressive acoustic emission changes observed across all wear stages.

Collectively, the most diagnostically powerful features - spectral centroid, skewness, and 0-500 Hz band power - exhibit clear separation even between adjacent wear stages (new vs. 25% worn), confirming that the proposed framework is sensitive to early-stage wear, not merely end-of-life discrimination. These results directly address the generalizability concern by demonstrating that the observed trends are consistent and progressive across intermediate wear stages, not only at the extremes.

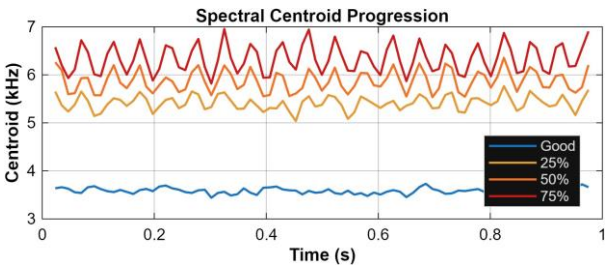

a)

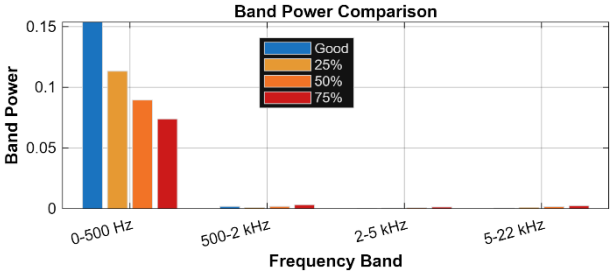

b)

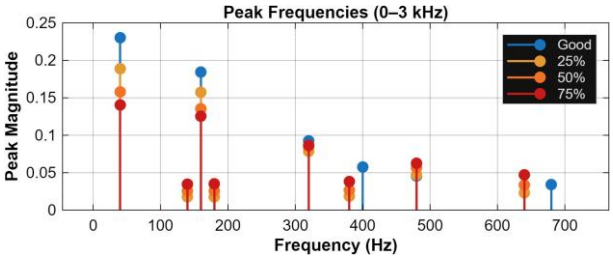

c)

Figure 6. Multi-stage FFT spectral feature comparison across four tool wear conditions (new, 25%, 50%, and 75% worn): (a) Spectral Centroid Progression showing monotonic shift from ~3.5 kHz to ~6.5 kHz; (b) Band Power Comparison confirming dominant energy redistribution in the 0–500 Hz band; (c) Peak Frequencies (0–3 kHz) showing progressive attenuation of harmonic magnitudes with increasing wear.

4. Conclusions

The findings of this study confirm that a single low-cost acoustic sensor, paired with disciplined signal processing, delivers reliable tool wear diagnostics in CNC steel milling without the sensor arrays or large datasets that competing approaches typically demand.

The cascaded *Kalman–FIR pipeline* was essential: the Kalman stage adaptively removed non-stationary shopfloor noise, while the FIR stage provided linear-phase frequency-selective smoothing — together exposing harmonic shifts that would otherwise be masked.

No single spectral feature alone separated the two wear states. Peak frequency remained fixed at 160 Hz (TPF) in both conditions. The decisive separation came from the joint behaviour of seven indicators: RMS amplitude (+35.9%), approximately 68% elevated band power in the 2–5 kHz sub-band, upward spectral centroid migration from ~3.5 kHz to ~6.5 kHz, broadening of dominant harmonic magnitudes across the 0–700 Hz range, increased spectral entropy, increased spectral flatness, and progressive attenuation of peak amplitudes at tooth-pass frequency harmonics — collectively forming an unambiguous acoustic fingerprint of progressive flank wear.

Based on the observed feature distributions, a spectral centroid exceeding ~5.0 kHz combined with a normalized spectral entropy above ~0.65 provides a sufficient binary criterion for distinguishing new from 75%-worn tool conditions under the tested cutting parameters.

Spectral entropy and flatness proved particularly transferable features: by quantifying distributional disorder rather than absolute frequency magnitudes, they remain effective across different spindle speeds and workpiece materials without recalibration. The consistency of spectral feature trends across five repeated experimental trials further confirms the repeatability of the proposed diagnostic approach under nominally identical cutting conditions.

End-to-end implementation in MATLAB and LabVIEW confirmed real-time viability — the full Kalman–FIR–FFT pipeline runs within a continuous monitoring loop, making it directly integrable into existing CNC controllers and accessible to small-to-medium enterprises where complex sensor infrastructure is not feasible.

Future work will validate the framework against physical milling trials under controlled wear progression, extending the multi-stage feature analysis to additional intermediate wear conditions and diverse workpiece materials. Efforts will also focus on developing automated threshold-based alarm logic directly from the spectral feature set, enabling fully autonomous, real-time tool condition alerts without reliance on external classification systems — advancing toward practical, scalable tool management aligned with Industry 4.0 requirements.

Acknowledgements

The author gratefully acknowledges Professor Dr. Almusawi Husam Abdulkareem for his guidance during the master's program and for introducing the foundations of research practice. Special thanks are extended to Professor Yakhshiev Sherali Namozovich at Navoi State University of Mining and Technologies for his valuable supervision and support throughout this study. The author also appreciates the assistance and contributions of colleagues and all who provided help during the research process.

References

[1] Vu VQ, Bui T-N and Tran M-Q (2025) AI-based tool wear prediction with feature selection from sound signal analysis. Front. Mech. Eng. 11:1608067. https://doi.org/10.3389/fmech.2025.1608067

[2] Munaro, R.; Attanasio, A.; Del Prete, A. Tool Wear Monitoring with Artificial Intelligence Methods: A Review. J. Manuf. Mater. Process. 2023, 7, 129. https://doi.org/10.3390/jmmp7040129

[3] Yin, Y., Wang, S. & Zhou, J. Multisensor-based tool wear diagnosis using 1D-CNN and DGCCA. Appl Intell 53, 4448–4461 (2023). https://doi.org/10.1007/s10489-022-03773-0

[4] Sherali Yakhshiev.; Ilkhom Egamberdiev.; Akmal Mamadiyarov.; Maruf Saibov.; and Nazokat Karimova.; Development of technology and methodology for monitoring the technical condition of metal cutting machines. E3S Web of Conferences 525, 05021 (2024). https://doi.org/10.1051/e3sconf/202452505021

[5] Nazokat Karimova.; Ulugbek Ochilov2.; Sherali Yakhshiev and Ilhom Egamberdiev.; Predictive maintenance of cutting tools using artificial neural networks. E3S Web of Conferences 471, 02021 (2024). https://doi.org/10.1051/e3sconf/202447102021

[6] Chen, M., Li, M., Zhao, L. et al. Tool wear monitoring based on the combination of machine vision and acoustic emission. Int J Adv Manuf Technol 125, 3881–3897 (2023). https://doi.org/10.1007/s00170-023-11017-9

[7] Kasiviswanathan, S.; Gnanasekaran, S.; Thangamuthu, M.; Rakkiyannan, J. Machine-Learning- and Internet-of-Things-Driven Techniques for Monitoring Tool Wear in Machining Process: A Comprehensive Review. J. Sens. Actuator Netw. 2024, 13, 53. https://doi.org/10.3390/jsan13050053

[8] Peng, Y., Song, Q., Wang, R. et al. Intelligent recognition of tool wear in milling based on a single sensor signal. Int J Adv Manuf Technol 124, 1077–1093 (2023). https://doi.org/10.1007/s00170-022-10404-y

[9] Karabacak, Y.E. Intelligent milling tool wear estimation based on machine learning algorithms. J Mech Sci Technol 38, 835–850 (2024). https://doi.org/10.1007/s12206-024-0131-z

[10] Cheng, Y., Gai, X., Guan, R. et al. Tool wear intelligent monitoring techniques in cutting: a review. J Mech Sci Technol 37, 289–303 (2023). https://doi.org/10.1007/s12206-022-1229-9

[11] González, D.; Alvarez, J.; Sánchez, J.A.; Godino, L.; Pombo, I. Deep Learning-Based Feature Extraction of Acoustic Emission Signals for Monitoring Wear of Grinding Wheels. Sensors 2022, 22, 6911. https://doi.org/10.3390/s22186911

[12] Peng, C.-Y.; Raihany, U.; Kuo, S.-W.; Chen, Y.-Z. Sound Detection Monitoring Tool in CNC Milling Sounds by K-Means Clustering Algorithm. *Sensors* **2021**, *21*, 4288. https://doi.org/10.3390/s21134288

[13] Wei, W.; Shang, Y.; Peng, Y.; Cong, R. Research Progress of Noise in High-Speed Cutting Machining. *Sensors* **2022**, *22*, 3851. https://doi.org/10.3390/s22103851

[14] Cheng, Y., Gai, X., Jin, Y. et al. A new method based on a WOA-optimized support vector

machine to predict the tool wear. Int J Adv Manuf Technol 121, 6439–6452 (2022). https://doi.org/10.1007/s00170-022-09746-4

[15] Jones, T., Cao, Y. Tool wear prediction based on multisensor data fusion and machine learning. *Int J Adv Manuf Technol* **137**, 5213–5225 (2025). https://doi.org/10.1007/s00170-025-15472-4

[16] Oshida, T., Murakoshi, T., Zhou, L. *et al.* Development and implementation of real-time anomaly detection on tool wear based on stacked LSTM encoder-decoder model. *Int J Adv Manuf Technol* **127**, 263–278 (2023). https://doi.org/10.1007/s00170-023-11497-9

[17] S. Liebich, J. Fabry, P. Jax and P. Vary, "Time-domain Kalman filter for active noise cancellation headphones," 2017 25th European Signal Processing Conference (EUSIPCO), Kos, Greece, 2017, pp. 593-597, doi: 10.23919/EUSIPCO.2017.8081276

[18] Lopes, Paulo & Piedade, Moisés. (2000). A Kalman filter approach to active noise control. European Signal Processing Conference. 2015.

[19] Aboutiman, A., Shams, R., Karimi, H. R., Ripamonti, F., Pawełczyk, M. Active noise control in encapsulated structures with non-minimum phase characteristics using a Kalman filter approach. J Sound Vib 615, 119187 (2025). https://doi.org/10.1016/j.jsv.2025.119187

[20] M. A. Hossin, M. Shil, V. Thanh and N. T. Son, "An Adjustable Window-Based FIR Filter and Its Application in Audio Signal De-Noising," *2018 3rd International Conference on Robotics and Automation Engineering (ICRAE)*, Guangzhou, China, 2018, pp. 248-252, doi: 10.1109/ICRAE.2018.8586723

[21] Harčarik, T., Bocko, J., Masláková, K. Frequency analysis of acoustic signal using the Fast Fourier Transformation in MATLAB. Procedia Eng 48, 199–204 (2012). https://doi.org/10.1016/j.proeng.2012.09.505

[22] Fang, X., Zheng, J. & Jiang, B. A rolling bearing fault diagnosis method based on vibro-acoustic data fusion and fast Fourier transform (FFT). *Int J Data Sci Anal* **20**, 2377–2386 (2025). https://doi.org/10.1007/s41060-024-00609-7

[23] D. E. Dimla, "Sensor signals for tool-wear monitoring in metal cutting operations," Int. J. Mach. Tools Manuf., vol. 40, pp. 1073–1098, 2000

[24] Y. Altintas, Manufacturing Automation, 2nd ed. Cambridge Univ. Press, 2012.

[25] Khasanov, S., Mardonov, U., Ongboyev, A., & Ismatov, M. M. (2024). Influence of a magnetic field on HSS tool wear/life and the intensity of external machining environments in turning. *International Journal of Mechatronics and Applied Mechanics*, (16), 163-170. https://doi.org/10.17683/ijomam/issue16.19

[26]] I. Inasaki, "Application of acoustic emission sensor for monitoring machining processes," Ultrasonics, vol. 36, pp. 273–281, 1998